Solar-Terrestrial Physics. 2025, vol. 11, iss. 3, pp. 13–21. DOI: 10.12737/stp-113202502. © 2025
L.S. Rakhmanova, M.O. Riazantseva, A.A. Khokhlachev, Y.I. Yermolaev, G.N. Zastenker. Published by INFRA-M Academic Publishing House

DOI: 10.12737/stp-113202502

Received March 10, 2025
Accepted May 05, 2025

FEATURES OF TURBULENT CASCADE DEVELOPMENT IN THE MAGNETOSHEATH DURING ICME

L.S. Rakhmanova
Space Research Institute RAS,
Moscow, Russia, rakhlud@gmail.com

M.O. Riazantseva
Space Research Institute RAS,
Moscow, Russia, orearm@gmail.com

A.A. Khokhlachev
Space Research Institute RAS,
Moscow, Russia, aleks.xaa@yandex.ru

Yu.I. Yermolaev
Space Research Institute RAS,
Moscow, Russia, yermol@cosmos.ru

G.N. Zastenker
Space Research Institute RAS,
Moscow, Russia, gzastenk@iki.rssi.ru

Abstract. Large-scale disturbances in the interplanetary medium are the main cause of the global perturbations inside Earth's magnetosphere. Transition region called magnetosheath is known to be located in front of the magnetosphere in which plasma and magnetic field properties, as well as their variations differ significantly from those in the solar wind. Particularly, plasma passage through the magnetosheath has been demonstrated to modify substantially features of the cascade of turbulent fluctuations of the solar wind, with the pattern of the modification being different for quiet and disturbed conditions in the interplanetary medium. In this study, we examine features of turbulent cascade formation in the magnetosheath during interplanetary manifestation of coronal mass ejection (ICME), by analyzing several cases of ICME interactions with the magnetosphere. The analysis is conducted by comparing magnetic field variations measured simultaneously in the solar wind and in the dayside magnetosheath by Wind, Cluster, THEMIS, and MMS spacecraft in 2016–2017. Interaction of ICME with the magnetosphere is shown to cause the least change in the fluctuation power if there is a compression region in front of it; on the opposite, when there is no compression region, the fluctuation power increases considerably. ICMEs that caused significant changes in the *Dst* index were determined to be accompanied by the least changes in the turbulent cascade in the magnetosheath, whereas the most significant modification of the turbulence features were observed during ICMEs which did not trigger substantial geomagnetic disturbances.

Keywords: solar wind, magnetosheath, turbulence, space plasma.

INTRODUCTION

It is known that the main sources of global magnetospheric disturbances are large-scale interplanetary disturbances [Yermolaev et al., 2015; Borovsky, Denton, 2006]. At the same time, geoeffectiveness of the solar wind (SW) and the relationship of geomagnetic disturbances with interplanetary medium parameters are usually studied using measurements in the vicinity of the L1 point, located 1.5 million km from Earth's orbit [Pallocchia et al., 2006; Boynton et al., 2012; Podladchikova, Petrukovich, 2012], and ignoring the processes in boundary layers of the magnetosphere. In front of the outer boundary of the magnetosphere — the magnetopause — there is always a bow shock (BS) and a transition region formed because supersonic and super-Alfvén SW streams flow around the magnetosphere. In the transition region, or magnetosheath (MSH), plasma and magnetic field characteristics change significantly — magnetic field lines are compressed, the magnetic field changes direction, plasma is compressed, slows down, and heats, as well as the fluctuation intensity of all parameters increases greatly. Processes in MSH depend on the relative position of BS and the interplanetary magnetic field: due to the presence of ions behind quasi-parallel BS, which are reflected from BS and then carried away by SW plasma to MSH, the amplitude of plasma parameter and magnetic field variations behind quasi-parallel BS is by an order of magnitude higher than behind quasi-perpendicular BS, and can reach the order of magnitude of the parameter itself [Greenstadt, 1972; Shevyrev, Zastenker, 2005]. Moreover, the temperature anisotropy that occurs on quasi-perpendicular BS leads to the development of a large number of instabilities and wave processes behind it [Schwartz et al., 1996; Lacombe, Belmont, 1995].

Despite the fact that there are general ideas about the global change in plasma and field characteristics behind BS, and it can, on average, be described by gas-dynamic and magnetohydrodynamic (MHD) models [Spreiter et al., 1966; Tóth et al., 2005] on scales comparable to the size of the magnetosphere (~10^5 km), the processes on smaller scales (~10^2–10^3 km) can only be reproduced by time-consuming hybrid and kinetic models (e.g. [Karimabadi et al., 2014; Palmroth et al., 2018]), which cannot be applied to space weather forecasting. Studies based on simultaneous measurements in front of and

behind BS show that the direction of the magnetic field directly in front of the magnetopause may differ from that recorded in SW [Šafránková et al., 2009; Pulinets et al., 2014]. In addition, recent studies indicate that during such geoeffective large-scale phenomena as Interplanetary Coronal Mass Ejections (ICMEs) there can also be mismatches between field directions in MSH and SW [Turc et al., 2017] on time scales of the order of an hour. Since IMF B_z is considered as the most important parameter of the interplanetary medium responsible for the dynamics of the magnetosphere, it is important to take into account the processes in MSH for a more correct understanding of solar-terrestrial relations.

On scales comparable to the proton gyroradius, kinetic effects play an important role in space plasma, energy dissipation begins, and the MHD description becomes inapplicable. The processes occurring on scales smaller than 10^3 km can be analyzed in terms of turbulent cascade characteristics. In recent years, a large amount of experimental data with high temporal resolution has significantly expanded the understanding of turbulence features in MSH (for example, [Zimbardo et al., 2010; Sahraoui et al., 2020; Rakhmanova et al., 2021]). For undisturbed SW plasma, the spectrum of turbulent magnetic field fluctuations has a universal form described by a power function with an exponent of –5/3 (Kolmogorov scaling) on scales larger than the ionic gyroradius (MHD scales). On scales of the order of the proton inertial length, the spectrum break and transition to kinetic scales occur on which the spectrum is also described by the power law with exponent α. According to statistical data, on average $\alpha=-(2.8\div3)$, whereas according to theoretical predictions α ranges from –7/3 [Schekochihin et al., 2009] to –8/3 [Boldyrev, Perez, 2012]. Most studies show that the characteristics of turbulent fluctuation spectra change at BS: Kolmogorov scaling on MHD scales is disrupted [Czaykowska et al., 2001; Huang et al., 2017; Rakhmanova et al., 2018a; Rakhmanova et al., 2024a] and the spectra can be described by the power law with an exponent of –1, typical of a set of incoherent waves or scales of energy pumping. On kinetic scales, some studies have demonstrated a significant steeping of fluctuation spectra behind BS [Rakhmanova et al., 2018b, 2024a], presumably caused by increased energy dissipation due to a large number of wave processes and instabilities characteristic of MSH.

Note also that turbulence characteristics depend on SW plasma type, determined largely by its solar source [Bruno et al., 2014; Riazantseva et al., 2019, 2020; Ervin et al., 2024]. Furthermore, it has been shown [Rakhmanova et al., 2024c; Rakhmanova et al., 2024b] that different turbulence types are characterized by different dynamics of turbulence properties behind BS, including different degrees of modification of the turbulent cascade in dayside MSH and the specific nature of its recovery during plasma propagation to MSH flanks.

Thus, the study into the features of the development of a turbulent cascade in MSH during disturbances in SW can provide insight into the processes occurring in the transition region during observation of potentially geoeffective phenomena in the interplanetary medium, and complement existing ideas about solar-terrestrial relations. In this paper, we have analyzed 15 cases of ICMEs recorded at Earth's orbit and changes in plasma turbulence characteristics when crossing BS in these periods. ICMEs are interplanetary coronal mass ejections that lead to the formation of large-scale magnetoplasma structures propagating in the interplanetary medium. If the propagation velocity of magnetoplasma structure from the Sun exceeds the velocity of surrounding SW plasma, a compression region (Sheath) can form in front of it, as in front of a piston, which features an increased plasma pressure (density and temperature) and fluctuation power. If the propagation velocity of the disturbance exceeds the local velocity of a fast MHD wave, an interplanetary shock is also formed in front of the piston. In Earth's orbit, ICME is identified by a set of plasma and magnetic field parameters [Yermolaev et al., 2009], as well as by ionic composition and energetic particle fluxes [Richardson, Cane, 2010]. ICME is characterized by an increase in the magnetic field compared to the surrounding SW, a significant decrease in temperature, an increase in velocity at the beginning of the event, and its decrease by the end of the event. Besides, there is often an increase in the relative content of alpha particles, as well as ions with large charges such as iron and oxygen. ICME is generally observed in two forms in Earth's orbit — Ejecta or magnetic cloud (MC). MC includes ICMEs that feature a quiet magnetic field of high amplitude without significant variations, with a smooth rotation of the magnetic field vector by a large angle, a significant decrease in temperature and proton density, and hence in the plasma parameter β — the ratio of thermal pressure to magnetic pressure [Burlaga, 1991]. The difference between ICMEs of these two types is probably due to different trajectories at which they are crossed by recording spacecraft (SC) [Yermolaev et al., 2009; Kilpua et al., 2017]. ICME formation, distribution, and internal structure are described in detail, for example, in the review [Kilpua et al., 2017]. For this work, we have taken events from the catalog [Yermolaev et al., 2009]; Ejecta and MC events were examined separately. Ejecta events without Sheath observed in front of ICME were considered separately from the events with Sheath, whereas Sheath was always recorded in MC. The periods corresponding directly to Sheaths were also studied independently. In addition, by analyzing the *Dst* index, we identified the Ejecta events that occurred in both SW and MSH, but without significant geomagnetic disturbances, and found characteristic changes in the turbulent cascade properties during these periods. We analyzed simultaneous measurements of turbulence characteristics in SW, using data from the Wind satellite; and in MSH, using data from any THEMIS, Cluster, MMS satellite. The analysis was carried out for 2016–2017, since this period corresponded to the descending phase of the solar cycle and to the observation of a sufficient number of geoeffective events in the interplanetary medium, and there is a large amount of available satellite data obtained in MSH.

1. DATA AND ANALYSIS METHOD

The time intervals corresponding to ICMEs have been selected from the catalog [Yermolaev et al., 2009; http://iki.rssi.ru/pub/omni/catalog/]. For all ICME observations in 2016–2017, we have determined the location of THEMIS, Cluster, and MMS satellites, as well as the availability of their measurements for the given time intervals, from [https://cdaweb.gsfc.nasa.gov/sp_phys/]. The location of a satellite inside MSH was found by analyzing the ion energy distribution, the proton density and velocity. We chose only the events during which the satellites were in the dayside MSH (X_{GSE}>5 R_E) and there were rapid satellite measurements of the magnetic field in MSH. We employed data from FGM instruments: on board THEMIS satellites [Auster et al., 2008] with a sampling rate of 4 vectors per second, on board Cluster satellites [Balogh et al., 2001] with a sampling rate of 5 vectors per second, on board MMS satellites with a sampling rate of 16 vectors per second (in a fast mode) [Russell et al., 2016]. With magnetic field measurements available for the selected event, we compared satellite measurements in MSH and SW. We used measurements of plasma parameters in SW with SWE [Ogilvie et al., 1995] at a temporal resolution of 92 s and of the magnetic field with MFI [Lepping et al., 1995] at a sampling rate of 11 vectors per second on board the Wind satellite in the vicinity of the libration point L1. Plasma parameters in MSH were analyzed using data from ESA/THEMIS [McFadden et al., 2008], CIS/Cluster [Rème et al., 2001] and FPI/MMS [Pollock et al., 2016]. We have selected 15 ICME events recorded in Earth's orbit.

To compare the data obtained in SW and MSH, it is necessary to correctly determine the time of plasma propagation between spacecraft. The propagation time was found from correlation analysis of time series of proton density from the Wind satellite and one of the satellites in MSH. For this purpose, density measurements were reduced to a general time grid with a resolution of 92 s, then a preliminary time shift $T_0=dX/|V_X|$ was calculated, where dX is the distance between satellites along the X_{GSE} axis; V_X is the average SW plasma velocity component along the X_{GSE} axis, measured by the Wind satellite during the event. Next, we calculated the density correlation coefficient for the time shift range [T_0–3600 s; T_0+3600 s]. The correlation coefficient was computed for an interval of 2 to 8 hrs, depending on the available data interval. The dT shift corresponding to the maximum of the correlation coefficient was determined, and the resulting value was selected as the time shift for the interval considered. Each dT value was manually checked against the visual coincidence between density fronts or magnetic field components on the two satellites and was adjusted if necessary. Figure 1 compares measurements from Wind SC in SW and from MMS-1 SC in MSH for the February 2–3, 2016 event. Panels *a*, *b* show proton density and velocity measurements; the left Y-axis represents the satellite in SW; the right one, the satellite in MSH. Panels *c*, *d* exhibit magnetic field magnitude and components in SW and MSH. The horizontal arrows above the top panel of the figure indicate SW types — before 22:00 there was a Sheath in front of ICME; from 22:00, the ICME itself, which belonged to the Ejecta type. The Wind data is shifted by 4380 s. The time variation in the proton density is clearly seen to coincide on the two satellites throughout the interval, as well as there are local inconsistencies in plasma structures, which usually emerge due to differences in their propagation velocities.

To identify the geomagnetic response to the event in question, we analyzed the *Dst* index from the Kyoto Observatory [https://wdc.kugi.kyoto-u.ac.jp/dstdir/]. Figure 1, *d* presents *Dst* values with a temporal resolution of 1 hr. The arrival of ICME is seen to be accompanied by a geomagnetic storm with minimum *Dst*=–57 nT. In this paper, the events were divided into those causing a significant response from the magnetosphere if they occurred with a change in *Dst* to less than –30 nT, and those that did not cause a significant geomagnetic response if *Dst* did not fall below –30 nT after the arrival of ICME.

For further analysis of the turbulence characteristics in this event, we have selected two intervals marked in Figure 1 with a gray fill: interval 1 refers to Sheath; and interval 2, to Ejecta. The intervals are taken according to their duration (~ 1 hr), as well as from considerations that the parameters are quasi-stationary, i.e. without significant density jumps or rotations of the magnetic field vector, which generally correspond to the intersection of discontinuities of various types. For each interval, the time shift was additionally adjusted manually.

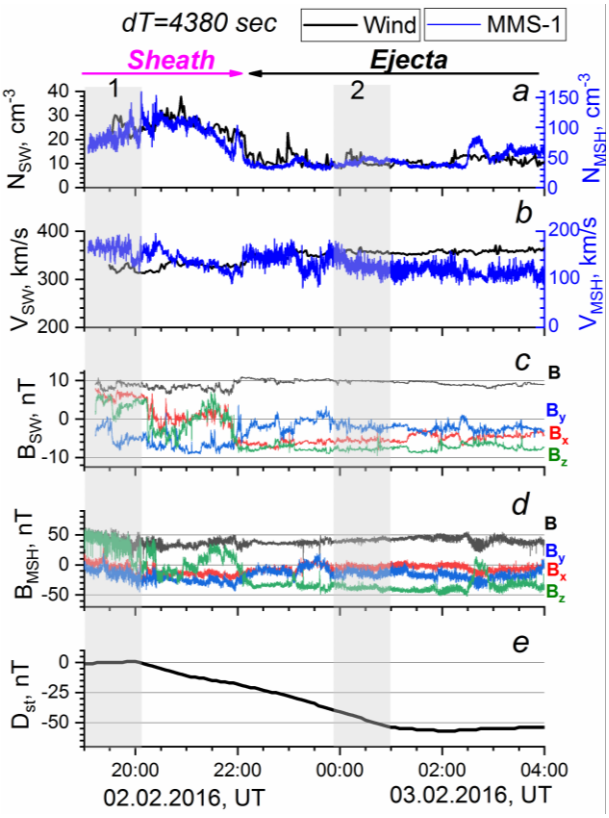

Figure 1. The February 2–3, 2016 event: proton density (*a*) and velocity (*b*) as measured by Wind in SW and by MMS-1 in MSH; magnetic field magnitude and components as measured by Wind in SW (*c*) and by MMS-1 in MSH (*d*); the *Dst* index (*e*)

For the selected intervals, turbulence characteristics in SW and MSH were found by Fourier analysis. Since the temporal resolution of magnetometers in the satellites in use varies, the intervals for calculating fluctuation spectra have different durations in SW and MSH. This difference is due to the use of Fourier analysis, which imposes a limit on the number of points in the spectrum. In this case, for the MMS-1 and Wind satellites the duration of the intervals is 68 and 50 min respectively. The intervals were chosen so that their centers coincide. Fourier spectra were computed for fluctuations of both the magnetic field vector (trace magnetic field fluctuation spectra) and the magnetic field magnitude. The magnetic field vector fluctuations are the sum of the incompressible (Alfvén) component of fluctuations, whereas magnetic field magnitude fluctuations represent the compression component. The contribution of the compression component of fluctuations to the cascade in SW is generally negligible, and turbulence is considered to be purely Alfvén [Schekochihin et al., 2009]. In MSH, the proportion of compression fluctuations becomes significant [Huang et al., 2017], which is an important feature of turbulence in this region.

Figure 2 illustrates the calculated spectra for the intervals marked in gray in Figure 1: panels *a*, *c* show interval 1 (Sheath); panels *b*, *d*, interval 2 (Ejecta). Panels *a*, *b* are spectra in SW; panels *c*, *d*, spectra in MSH. Note that on the scales in SW considered, the noise of MFI can make a significant contribution to the spectra

For the obtained spectra, two scales, separated by a break, are pronounced: MHD and kinetic. On these scales, the spectra were linearly approximated on a logarithmic scale for each range, and the exponent of the

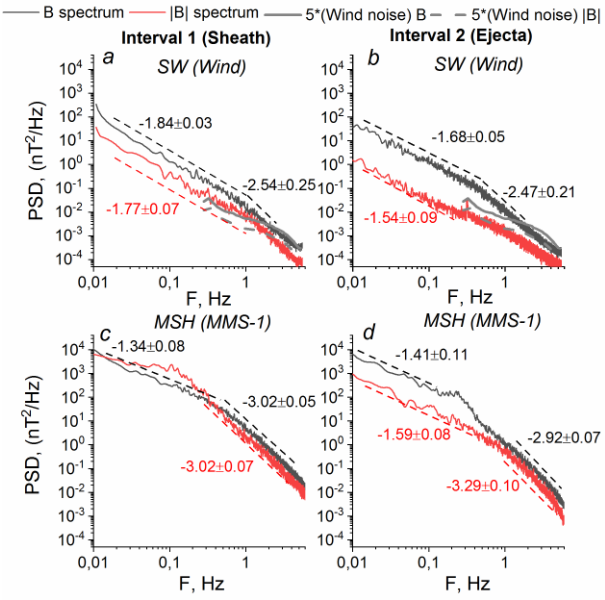

Figure 2. Spectra (solid lines) of trace magnetic field (black curves) and magnitude (red curves) fluctuations in SW (*a*, *b*) and MSH (*c*, *d*) for intervals 1 (*a*, *c*) and 2 (*b*, *d*) in Figure 1, as well as the results of approximation of the spectra (dashed lines). Gray lines in panels *a*, *b* are MFI's noise spectra multiplied by a factor of 5: solid lines are trace magnetic field fluctuation spectra; dashed lines are magnetic field magnitude fluctuation spectra.

power law (slope) of the spectrum was found. In some cases, such an approximation is impossible due to the presence of a peak in the spectrum (the fluctuation spectrum of the magnetic field magnitude in Figure 2, *c*) or because the noise level is reached (the spectrum of magnetic field magnitude fluctuations in Figure 2, *b*).

For most events in SW, analyzed both in this paper and in earlier statistical studies [Woodham et al., 2018], the spectrum breaks at frequencies above 0.1 Hz. In this work, we have chosen the frequency range 0.095–0.105 Hz to estimate the intensity of fluctuations on MHD scales. For each spectrum, we determined the intensity of magnetic field vector and magnitude fluctuations in SW and MSH.

Figure 2 indicates that in SW during the Sheath period the MHD-scale spectra are slightly steeper (~–1.8) than the Kolmogorov spectrum with a slope of –5/3. This slope is typical for Sheath regions [Riazantseva et al., 2024]. During the Ejecta period, the spectra have a slope close to the Kolmogorov one on MHD scales. For interval 1 inside Sheath, the spectrum of magnetic field magnitude fluctuations has a scaling close to that of the field vector fluctuation spectrum, while the intensity of magnetic field vector and magnitude fluctuations differs three times. SW is generally characterized by a large difference in power (by 10 or more times) due to the dominant contribution of Alfvén incompressible fluctuations, which is observed, for example, for the Ejecta period (see Figure 2, *b*) having the power of the compression component ~40 times lower. However, Sheath exhibits a high density, which causes an increase in the proportion of the compressible component of fluctuations. On kinetic scales, the fluctuation spectra have slopes close to –8/3, given in a number of theoretical descriptions of turbulence.

In MSH, the spectra are characterized by flattening on MHD scales and a deviation of scaling from the Kolmogorov scale for magnetic field vector fluctuations. At the same time, during the Sheath period there is a peak in the spectrum of field magnitude fluctuations; and during the Ejecta period, in the field vector spectrum. The frequency range in which the peak was observed was excluded from consideration. It is beyond the scope of this paper to discuss the nature of these peaks. Such peaks are typically caused by wave processes in MSH due to temperature anisotropy, and the type of process depends on external conditions [Schwartz et al., 1996; Lacombe, Belmont, 1995]. Both intervals are typified by steeping of the spectra on kinetic scales. For the Sheath interval, the intensity of magnetic field vector and magnitude fluctuations is close on both MHD and kinetic scales, which indicates a significant contribution of compression fluctuations to the cascade. For the Ejecta interval, the proportion of compression fluctuations in MSH on MHD scales, as well as in SW, is much smaller than the proportion of Alfvén fluctuations, whereas their contribution increases on kinetic scales.

The break frequency of spectra is also an important feature of turbulence since it is believed that the scale on which the break appears is related to the mechanism

of energy dissipation and plasma heating. However, identifying this scale requires significant statistics, and even if any, the scale is still not clearly defined (see, e.g., [Woodham et al., 2018]). In this paper, the statistics does not allow us to reliably determine which scale is typical of the spectrum break, so this problem was left aside.

A total of 47 intervals have been identified for 15 ICME events, divided according to the type of ICME and the intensity of geomagnetic disturbances they triggered into the following groups: 1) Ejecta ICME before which there was a compression region and after which Dst<–30 nT, i.e. there was a geomagnetic disturbance (GS) — Ejecta/Sh/GS; 2) Ejecta ICME before which there was a compression region and after which Dst>–30 nT, i.e. there was no significant geomagnetic disturbance — Ejecta/Sh/noGS; 3) Ejecta ICME before which no compression region was observed and Dst>–30 nT — Ejecta/noSh; 4) Sheath after which Dst<–30 nT — Sh; 5) ICME of MC type after which Dst<–30 nT — MC. The number of intervals of each type and the presence/absence of the magnetospheric response to the event, as well as averages of IMF B_z and SW plasma velocity for the selected group of events are listed in Table. According to the results of statistical studies [Rakhmanova et al., 2024a, b], the disturbed periods in SW and in particular the period of ICME passage are characterized by a significant modification of the turbulent cascade throughout the dayside MSH, regardless of the satellite location relative to the magnetopause and BS. Therefore, in this work we do not separate intervals near the boundaries and in the middle of MSH. There is also no separation according to the type of the BS behind which the measurements were made.

Using the statistics obtained, we have analyzed the changes when crossing BS: 1) the power of PSD fluctuations on MHD scales; 2) the degree of compression (compression coefficient) on MHD scales $CC=PSD_{|B|}/PSD_B$, where $PSD_{|B|}$ is the intensity of magnetic field magnitude spectrum fluctuations, PSD_B is the power of magnetic field vector fluctuations; 3) slopes P_1 and P_2 on MHD and kinetic scales respectively for each interval type. The results of the analysis are presented in the next section.

2. RESULTS

Figure 3 compares slopes of magnetic field vector fluctuation spectra in SW and MSH on MHD (*a*) and kinetic (*b*) scales for events of different types. Magnetic field magnitude fluctuations in SW are adversely affected by MFI noise, which hinders identification of slopes of spectra of these fluctuations for kinetic scales. Accordingly, the scaling of fluctuations was compared only for the magnetic field vector. Black dashed lines indicate the equality of the slopes of the spectra in front of and behind BS, i.e. preservation of scaling when entering into MSH. Blue dashed lines show the model slopes specific to each scale range. For the intervals related to Sheath and MC, the spectra on MHD scales in SW are close to the Kolmogorov spectra. For other SW types, there is a wide spread of slopes. In MSH, most spectra have slopes lower in magnitude than in SW and as described in theories. Note that the number of points in Figure 3 may be smaller than the number of intervals in Table since in a large number of cases wave phenomena are observed in MSH and it is impossible to approximate the spectra on MHD scales. In the fourth column of Table is the number of cases of observation of well-defined peaks in the spectra of magnetic field vector fluctuations in MSH. The most common wave phenomena are observed for Ejecta/Sh/noGS events — 10 of 13 cases, as well as for Ejecta/noSh events — 10 of 13 cases. Thus, for ICMEs that did not produce a significant magnetospheric response, intense wave activity is observed in 76 % of cases in the dayside MSH. For the events that evoked a significant magnetospheric response, wave processes in MSH occurred in 38 % of cases.

For Ejecta/Sh/GS events, slopes of spectra on MHD scales in MSH correspond to those measured in SW, both for the Kolmogorov scaling and for deviation from it in SW. For other events, there is no connection between the slopes of the spectra in the two regions.

On kinetic scales, the fluctuation spectra in MSH have, on average, a slope larger in magnitude than that in SW, which is typical of MSH plasma. The smallest slope

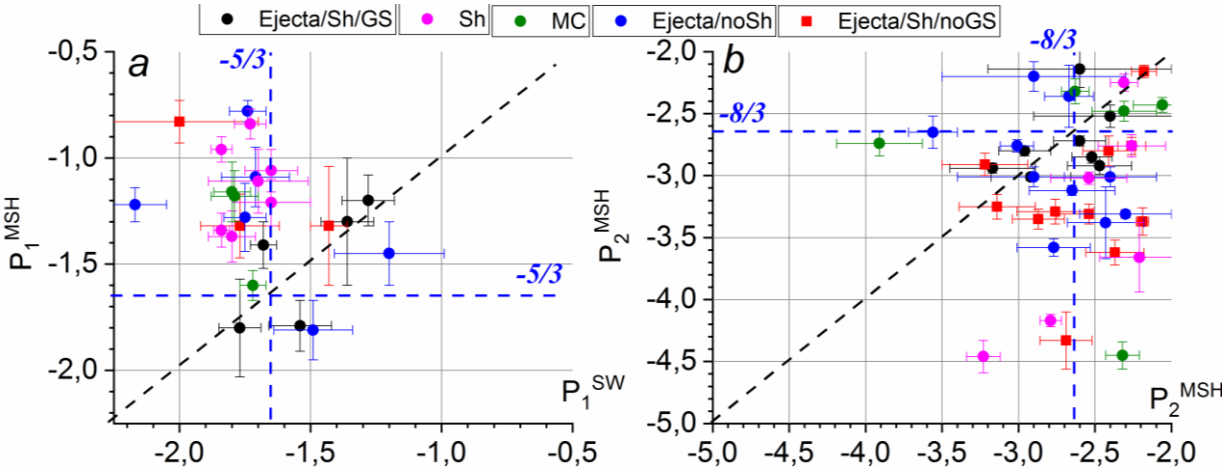

Figure 3. Slope of magnetic field vector fluctuation spectrum in MSH as function of the slope in SW on MHD scales (*a*) and on kinetic scales (*b*)

Types of intervals considered and their characteristics

Type	Number of intervals	Magnetospheric response	Number of intervals with peak in MSH	Average B_z in SW, nT	Average V in SW, km/s
Ejecta/Sh/GS	8	+	5	–5.3±3.3	355±4
Ejecta/Sh/noGS	13	–	10	3.7±4.1	420±64
Ejecta/noSh	13	–	10	1.2±2.1	382±42
Sh	8	+	2	0.7±3.2	422±109
MC	5	+	1	–6.3±5.7	473±100

change when plasma enters into MSH is observed for Ejecta/Sh/GS events; the largest one, for Ejecta/Sh/noGS, Ejecta/noSh, and Sh events. Interestingly, for four of five MC events, there is a spread of slopes in SW, whereas in MSH the slope values are close to –8/3. Such a change may indicate that the cascade of turbulent fluctuations can collapse and form again behind BS, not only for MHD, as suggested in [Huang et al., 2017], but also for kinetic scales. Yet, it is impossible to answer this question unambiguously in the framework of this work due to the limited statistics on MC. For one of the five events, the slope on kinetic scales is close to –4.5, which is typical for observing the wave processes or local coherent structures such as Alfvén vortices [Alexandrova et al., 2008].

Figure 4 compares averages and standard deviations of changes in slopes of fluctuation spectra at BS on MHD (*a*) and kinetic (*b*) scales for the ICME types considered. The slope change is defined as $P_{1,2} = \left(P_{1,2}^{\mathrm{MSH}} - P_{1,2}^{\mathrm{SW}}\right) / P_{1,2}^{\mathrm{SW}}$, where indices 1 and 2 relate to MHD and kinetic scales respectively. In the case of flatter fluctuation spectra characteristic of MSH, $\Delta P<0$; in the case of fluctuation spectrum steeping at BS, $\Delta P>0$. Despite the large standard deviations of the values, we can see that different ICME types have their own peculiarities in changing the scaling behind BS. The most significant difference is observed for the Ejecta events that cause and do not cause magnetospheric disturbances. In the former case, there is the smallest change in the scaling of fluctuation spectra on both MHD and kinetic scales. In the latter, most events show an increase in wave activity and energy dissipation rates in MSH.

The magnetic field vector fluctuation intensity in MSH is plotted versus the corresponding intensity in SW, measured on MHD scales, in Figure 5, *a*. Averages and standard deviations of variation in the spectral power $\log(PSD_{\mathrm{MSH}}/\ /PSD_{\mathrm{SW}})$ are presented in Figure 4, *c*. For MC and Ejecta/Sh/GS, crossing of BS is seen to occur with an increase in the intensity of fluctuations by two orders of magnitude. Sheath and Ejecta/Sh/noGS are characterized by a less pronounced increase in fluctuations — by 1–2 orders of magnitude. The most significant enhancement of fluctuations, in some cases by more than three orders of magnitude, is recorded during Ejecta/noSh periods.

One of the main differences between MSH plasma and undisturbed SW plasma is an increase in the proportion of the compression component of fluctuations behind BS.

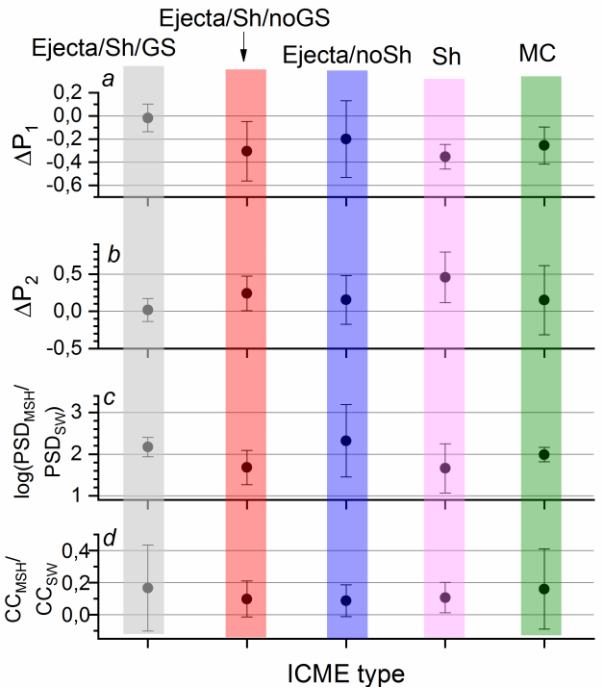

Figure 4. Average and standard deviation of changes in slopes P_1 (*a*) and P_2 (*b*), as well as changes in the spectral power of fluctuations on MHD scales (*c*) and the compression coefficient (*d*) for ICMEs of different types

Figure 5, *b* compares compression coefficients in SW and MSH for all types of intervals considered. Averages and standard deviations for ICMEs of different types are shown in Figure 4, *d*. It is clearly seen that in SW the power of the compression component of magnetic field fluctuations for most events is ten times lower than the power of the Alfvén component ($CC_{\mathrm{SW}}<0.1$), which is typical of SW. At the same time, the proportion of compression fluctuations is, on average, higher for Sheath regions, which is natural for regions of compressed plasma. There is no significant difference in the compression coefficient for Ejecta intervals of different types. In MSH, the CC_{MSH} coefficient is, on average, higher than in SW, and the proportion of the compressible component is usually comparable to that of the Alfvén one. There is no clear relationship between the compressibilities of fluctuations in SW and MSH: on average, the compressibility increases by one order of magnitude for all the ICME types considered. Thus, an increase in compressibility does not seem to play a role in the difference in the dynamics of the turbulent cascade behind BS for ICMEs of different types and in the difference in the geomagnetic response to them.

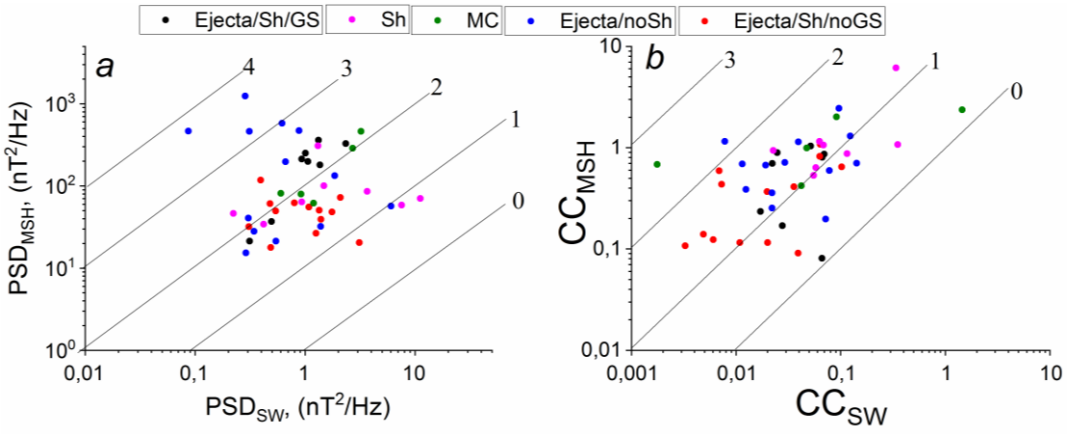

Figure 5. Intensity of magnetic field vector fluctuations in MSH as a function of corresponding intensity in SW for MHD scales (*a*); the compression coefficient in MSH versus that in SW for different ICME types (*b*); lines indicate an increase in intensity (*a*) and degree of compression (*b*) 10^n times; *n* is given near the corresponding line

3. DISCUSSION AND CONCLUSIONS

In this paper, by analyzing simultaneous measurements of turbulence characteristics in the solar wind and in the dayside magnetosheath, we have examined the difference in turbulent cascade forming behind the bow shock for 15 ICME events of various types and varying degrees of geoefficiency. The following has been shown.

1. The most pronounced change in the scaling of the turbulent cascade on both MHD and kinetic scales is observed during Ejecta ICMEs, which are not accompanied by a significant magnetospheric response (*Dst*>–30 nT); it is not important whether there is or is not a Sheath in front of ICME; during these events behind BS, wave activity on inertial scales increases considerably, and the energy dissipation rate is enhanced.

2. The least pronounced change in the scaling of the turbulent cascade on both MHD and kinetic scales is typical for Ejecta regions with Sheath in front of them, causing significant disturbances of the magnetosphere (*Dst*<–30 nT).

3. Ejecta events without Sheath occur with the greatest enhancement of MHD-scale fluctuations at BS, which can be as large as four orders of magnitude.

4. The degree of compressibility of fluctuations varies on average by one order of magnitude behind BS, regardless of ICME type and for different magnetospheric responses to ICME.

The data on the change in scaling of fluctuations upon plasma entry into MSH agrees, on average, with the data obtained earlier in statistical studies [Czaykowska et al., 2001; Huang et al., 2017; Rakhmanova et al., 2024a, b]: there is a deviation of scaling from the Kolmogorov one on MHD scales and steeping of spectra on kinetic scales. However, this paper demonstrates an important difference between events that had the same type, i.e. a solar source, but were followed by a different response from the magnetosphere.

It should be noted that geoeffectiveness of Ejecta ICME has a well-explained relationship with IMF B_z (see Table): the events that cause a significant magnetospheric response are characterized by a pronounced southern orientation of the interplanetary magnetic field. Nonetheless, according to statistical analysis [Rakhmanova et al., 2024a], average B_z does not clearly affect the change in turbulence characteristics at BS. In this work, we have also analyzed the relationships of changes in the turbulence parameters at BS with the SW plasma and magnetic field parameters, in particular with the plasma velocity, and have found no dependences in ICME events. A significant increase in the intensity of fluctuations on MHD scales during Ejecta events that did not have a compression region in front of them and were not followed by a significant magnetospheric response, as well as the frequent observation of pronounced wave processes during these periods suggest that the energy of fluctuations coming from SW was converted into MHD waves. An increase in dissipation (steeping of fluctuation spectra on kinetic scales) characteristic of these periods also indicates the appearance of excess energy in the cascade, which is redistributed from large scales to smaller ones through the cascade. Intensification of wave processes is also observed during Ejecta periods with Sheath, which did not lead to significant magnetospheric disturbances, despite the evidence for greater geoeffectiveness of such events [Yermolaev et al., 2015].

Such features in the formation of the turbulent cascade behind BS suggest that not only global reconnection processes at the magnetopause, which are determined by the direction of the interplanetary magnetic field and SW dynamic pressure and are often indicated as the dominant process in solar-terrestrial relations, but also energy transfer processes through the cascade (e.g., [D'Amicis et al., 2020]) and their changes near BS, which may be specific to SW streams of different types, contribute to the geoeffectiveness of various phenomena in the interplanetary medium. This contribution requires more detailed research in order to build more accurate models of solar-terrestrial relations.

The work was carried out under the Government assignment from IKI RAS on the theme “PLASMA”.

REFERENCES

Alexandrova O., Lacombe C., Mangeney A. Spectra and anisotropy of magnetic fluctuations in the Earth's magnetosheath: Cluster observations. *Ann. Geophys*. 2008, vol. 26, iss. 11, pp. 3585–3596. DOI: 10.5194/angeo-26-3585-2008.

Auster H.U., Glassmeier K.H., Magnes W., Aydogar O., Baumjohann W., Constantinescu D., et al. The THEMIS Fluxgate Magnetometer. *Space Sci. Rev*. 2008, vol. 141, pp. 235–264. DOI: 10.1007/s11214-008-9365-9.

Balogh A., Carr C.M., Acuna M.H., Dunlop M.W., Beek T.J., Brown P., et al. The Cluster Magnetic Field Investigation: Overview of in-flight performance and initial results. *Ann. Geophys*. 2001, vol. 19, pp. 1207–1217. DOI: 10.5194/angeo-19-1207-2001.

Boldyrev S., Perez J.C. Spectrum of kinetic Alfven turbulence. *Astrophys. J. Lett*. 2012, vol. 758, no. 2, 5 p. DOI: 10.1088/ 2041-844 8205/758/2/L44.

Borovsky J.E., Denton M.H. The differences between CME-driven storms and CIR-driven storms. *J. Geophys. Res*. 2006, vol. 111, A07S08.

Boynton R.J., Balikhin M.A., Billings S.A., Sharma A.S., Amariutei O.A. Data derived NARMAX *Dst* model. *Ann. Geophys*. 2012, vol. 29, iss. 6, pp. 965–971. DOI: 10.5194/angeo-29-965-2011.

Bruno R., Trenchi L., Telloni D. Spectral slope variation at proton scales from fast to slow solar wind. *Astrophys. J. Lett*. 2014, vol. 793, L15.

Burlaga L.F. Magnetic clouds. *Physics of the Inner Heliosphere*: vol. 2. Eds R. Schwenn and E. Marsch. Springer-Verlag, 1991, p. 1. DOI: 10.1007/978-3-642-75364-0_1.

Czaykowska A., Bauer T.M., Treumann R.A., Baumjohann W. Magnetic field fluctuations across the Earth's bow shock. *Ann. Geophys*. 2001, vol. 19, iss. 3, pp. 275–287. DOI: 10.5194/angeo-19-275-2001.

D'Amicis R., Telloni D., Bruno R. The effect of solar-wind turbulence on magnetospheric activity. *Front. Phys*. 2020, vol. 8, 604857. DOI: 10.3389/fphy.2020.604857.

Ervin T., Jaffarove K., Badman S.T., Huang J., Rivera Ye.J., Bale S.D. Characteristics and source regions of slow Alfvénic solar wind observed by Parker Solar Probe. *Astrophys. J*. 2024, vol. 975, no. 2, 156. DOI: 10.3847/1538-4357/ad7d00.

Greenstadt E.W. Binary index for assessing local bow shock obliquity. *J. Geophys. Res*. 1972, vol. 77, pp. 5467–5479. DOI: 10.1029/JA077i028p05467.

Huang S.Y., Hadid L.Z., Sahraoui F., Yuan Z.G., Deng X.H. On the existence of the Kolmogorov inertial range in the terrestrial magnetosheath turbulence. *Astrophys. J. Lett*. 2017, vol. 836, no. 1, L10. DOI: 10.3847/2041-8213/836/1/L10.

Karimabadi H., Roytershteyn V., Vu H.X., Omelchenko Y.A., Scudder J., Daughton W., et al. The link between shocks, turbulence, and magnetic reconnection in collisionless plasmas. *Phys. Plasmas*. 2014, vol. 21, 062308. DOI: 10.1063/ 1.4882875.

Kilpua E., Koskinen H.E.J., Pulkkinen T.I. Coronal mass ejections and their sheath regions in interplanetary space. *Living Rev. Solar Phys*. 2017, vol. 14, article number 5. DOI: 10.1007/s41116-017-0009-6.

Lacombe C., Belmont G. Waves in the Earth's magnetosheath: observations and interpretations. *Adv. Space Res*. 1995, vol. 15, pp. 329–340. DOI: 10.1016/0273-1177(94)00113-F.

Lepping R.P., Acũna M.H., Burlaga L.F., Farrell W.M., Slavin J.A., Schatten K.H., et al. The WIND Magnetic Field Investigation. *Space Sci Rev*. 1995, vol. 71, pp. 207–229. DOI: 10.1007/BF00751330.

McFadden J.P., Carlson C.W., Larson D., Ludlam M., Abiad R., Elliott B., et al. The THEMIS ESA plasma instrument and in-flight calibration. *Space Sci. Rev*. 2008, vol. 141, pp. 277–302. DOI: 10.1007/s11214-008-9440-2.

Ogilvie K.W., Chornay D.J., Fritzenreiter R.J., Hunsaker F., Keller J., Lobell J., et al. SWE, a comprehensive plasma instrument for the WIND spacecraft. *Space Sci Rev*. 1995, vol. 71, pp. 55–77. DOI: 10.1007/BF00751326.

Pallocchia G., Amata E., Consolini G. Geomagnetic *Dst* index forecast based on IMF data only. *Ann. Geophys*. 2006, vol. 24, pp. 989–999. DOI: 10.5194/angeo-24-989-2006.

Palmroth M., Ganse U., Pfau-Kempf Y., Battarbee M., Turc L., Brito T., et al. Vlasov methods in space physics and astrophysics. *Living Reviews in Computational Astrophysics*. 2018, vol. 4, article number 1. DOI: 10.1007/s41115-018-0003-2.

Podladchikova T.V., Petrukovich A.A. Extended geomagnetic storm forecast ahead of available solar wind measurements. *Space Weather*. 2012, vol. 10, S07001. DOI: 10.1029/2012 SW000786.

Pollock C., Moore T., Jacques A., Burch J., Gliese U., Saito Y., et al. Fast Plasma Investigation for Magnetospheric Multiscale. *Space Sci. Rev*. 2016, vol. 199, pp. 331–406. DOI: 10.1007/s11214-016-0245-4.

Pulinets M.S., Antonova E.E., Riazantseva M.O., Znatkova S.S., Kirpichev I.P. Comparison of the magnetic field before the subsolar magnetopause with the magnetic field in the solar wind before the bow shock. *Adv. Space Res*. 2014, vol. 54, pp. 604–616. DOI: 10.1016/j.asr.2014.04.023.

Rakhmanova L.S., Riazantseva M.O., Zastenker G.N., Verigin M.I. Effect of the magnetopause and bow shock on characteristics of plasma turbulence in the Earth's magnetosheath. *Geomagnetism and Aeronomy*. 2018a, vol. 58, pp. 718–727. DOI: 10.1134/S0016793218060129.

Rakhmanova L., Riazantseva M., Zastenker G., Verigin M. Kinetic scale ion flux fluctuations behind the quasi-parallel and quasi-perpendicular bow shock. *J. Geophys. Res.: Space Phys*. 2018b, vol. 123, pp. 5300–5314. DOI: 10.1029/ 2018JA025179.

Rakhmanova L., Riazantseva M., Zastenker G. Plasma and magnetic field turbulence in the Earth's magnetosheath at ion scales. *Front. Astron. Space Sci*. 2021, vol. 7, 616635. DOI: 10.3389/fspas.2020.616635.

Rakhmanova L., Khokhlachev A., Riazantseva M., Yermolaev Y., Zastenker G. Modification of the turbulence properties at the bow shock: Statistical results. *Front. Astron. Space Sci*. 2024a, vol. 11, 1379664. DOI: 10.3389/fspas.2024.1379664.

Rakhmanova L., Khokhlachev A., Riazantseva M., Yermolaev Y., Zastenker G. Changes in and recovery of the turbulence properties in the magnetosheath for different solar wind streams. *Universe*. 2024b, vol. 10, no. 5, 194. DOI: 10.3390/universe10050194.

Rakhmanova L., Khokhlachev A., Riazantseva M., Yermolaev Y., Zastenker G. Turbulence development behind the bow shock during disturbed and undisturbed solar wind. *Sol.-Terr. Phys*. 2024c, vol. 10, no. 2, pp. 13–25. DOI: 10.12737/ stp-102202402.

Rème H., Aoustin C., Bosqued J.M., Dandouras I., Lavraud B., Sauvaud J.A., et al. First multispacecraft ion measurements in and near the Earth's magnetosphere with the identical Cluster Ion Spectrometry (CIS) experiment. *Ann. Geophys*. 2001, vol. 19, pp. 1303–1354. DOI: 10.5194/angeo-19-1303-2001.

Riazantseva M.O., Rakhmanova L.S., Zastenker G.N., Yermolaev Yu.I., Lodkina I.G., Chesalin L.S. Small-scale plasma fluctuations in fast and slow solar wind streams. *Cosmic*

Res. 2019, vol. 57, no. 6, pp. 434–442. DOI: 10.1134/S0010952519060078.

Riazantseva M.O., Rakhmanova L.S., Yermolaev Yu.I., Lodkina I.G., Zastenker G.N., Chesalin L.S. Characteristics of turbulent solar wind flow in plasma compression regions. *Cosmic Res*., 2020, vol. 58, no. 6, pp. 468–477. DOI: 10.1134/S001 095252006009X.

Riazantseva M.O., Treves T.V., Khabarova O., Rakhmanova L.S., Yermolaev Yu.I., Khokhlachev A.A. Linking turbulent interplanetary magnetic field fluctuations and current sheets. *Universe*. 2024, vol. 10, no. 11, 417. DOI: 10.3390/ universe10110417.

Richardson I.G., Cane H.V. Near-Earth interplanetary coronal mass ejections during solar cycle 23 (1996–2009): catalog and summary of properties. *Solar Phys*. 2010, vol. 264, pp. 189–237. DOI: 10.1007/s11207-010-9568-6.

Russell C.T., Anderson B.J., Baumjohann W., Bromund K.R., Dearborn D., Fischer D., et al. The Magnetospheric Multiscale Magnetometers. *Space Sci Rev*. 2016, vol. 199, pp. 189–256. DOI: 10.1007/s11214-014-0057-3.

Šafránková J., Hayosh M., Gutinska O., Němeček Z., Přech L. Reliability of prediction of the magnetosheath B_z component from the interplanetary magnetic field observations. *J. Geophys. Res*. 2009, vol. 114, A12213. DOI: 10.1029/2009A014552.

Sahraoui F., Hadid L., Huang S. Magnetohydrodynamic and kinetic scale turbulence in the near-Earth space plasmas: A (short) biased review. *Rev. Mod. Phys*. 2020, vol. 4, article number 4. DOI: 10.1007/s41614-020-0040-2.

Schekochihin A.A., Cowley S.C., Dorland W., Yermolaev Yu.I., Lodkina I.G., Chesalin L.S. Astrophysical gyrokinetics: Kinetic and fluid turbulent cascades in magnetized weakly collisional plasmas. *Astrophys. J. Suppl*. 2009, vol. 182, pp. 310–377. DOI: 10.1088/0067-0049/182/1/310.

Schwartz S.J., Burgess D., Moses J.J. Low-frequency waves in the Earth's magnetosheath: Present status. *Ann. Geophys*. 1996, vol. 14, pp. 1134–1150. DOI: 10.1007/s00585-996-1134-z.

Shevyrev N.N., Zastenker G.N. Some features of the plasma flow in the magnetosheath behind quasi-parallel and quasi-perpendicular bow shocks. *Planet. Space Sci*. 2005, vol. 53, pp. 95–102. DOI: 10.1016/j.pss.2004.09.033.

Spreiter J.R., Summers A.L., Alksne A.Y. Hydromagnetic flow around the magnetosphere. *Planet. Space Sci*. 1966, vol. 14, pp. 223–253.

Turc L., Fontaine D., Escoubet C.P., Kilpua E.K.J., Dimmock A.P. Statistical study of the alteration of the magnetic structure of magnetic clouds in the Earth's magnetosheath. *J. Geophys. Res.: Space Phys*. 2017, vol. 122, pp. 2956–2972. DOI: 10.1002/2016JA023654.

Tóth G., Sokolov I., Gombosi T., Chesney D., Clauer C.R., De Zeeuw D.L., et al. Space Weather Modeling Framework: A new tool for the space science community. *J. Geophys. Res*. 2005, vol. 110, A12226. DOI: 10.1029/2005 JA011126.

Woodham L.D., Wicks R.T., Verscharen D., Owen C.J. The role of proton cyclotron resonance as a dissipation mechanism in solar wind turbulence: A statistical study at ion-kinetic scales. *Astrophys. J*. 2018, vol. 856, no. 1, 49. DOI: 10.3847/1538-4357/aab03d.

Yermolaev Y.I., Nikolaeva N.S., Lodkina I.G., Yermolaev M.Y. Catalog of large-scale solar wind phenomena during 1976–2000. *Cosmic Res*. 2009, vol. 47, pp. 81–94. DOI: 10.1134/ S0010952509020014.

Yermolaev Y.I., Lodkina I.G., Nikolaeva N.S., Yermolaev M.Y. Dynamics of large-scale solar-wind streams obtained by the double superposed epoch analysis. *J. Geophys. Res.: Space Phys*. 2015, vol. 120, pp. 7094–7106. DOI: 10.1002/ 2015JA021274.

Zimbardo G., Greco A., Sorriso-Valvo L., Perri S., Vörös Z., Aburjania G., et al. Magnetic turbulence in the geospace environment. *Space Sci. Rev*. 2010, vol. 156, pp. 89–134. DOI: 10.1007/s11214-010-9692-5.

URL: http://iki.rssi.ru/pub/omni/catalog/ (accessed April 8, 2025).

URL: https://cdaweb.gsfc.nasa.gov/sp_phys/ (accessed April 8, 2025).

URL: https://wdc.kugi.kyoto-u.ac.jp/dstdir/ (accessed April 8, 2025).

The paper is based on material presented at the 20th Annual Conference on Plasma Physics in the Solar System, February 10–14, 2025, Space Research Institute of the Russian Academy of Sciences, Moscow, Russia.

Original Russian version: Rakhmanova L.S., Riazantseva M.O., Khokhlachev A.A., Yermolaev Y.I., Zastenker G.N., published in Solnechno-zemnaya fizika. 2025, vol. 11, no. 3, pp. 16–25. DOI: 10.12737/szf-113202502.

How to cite this article

Rakhmanova L.S., Riazantseva M.O., Khokhlachev A.A., Yermolaev Y.I., Zastenker G.N. Features of turbulent cascade development in the magnetosheath during ICME. *Sol.-Terr. Phys*. 2025, vol. 11, iss. 3, pp. 13–21. DOI: 10.12737/stp-113202502.